Low energy collective modes of deformed superfluid nuclei within the finite amplitude method

Nobuo Hinohara,[1,2,3] Markus Kortelainen,[4,2] and Witold Nazarewicz[2,5,6]

[1] *Department of Physics and Astronomy, University of North Carolina, Chapel Hill, North Carolina, 27599-3255, USA*
[2] *Department of Physics and Astronomy, University of Tennessee, Knoxville, Tennessee, 37996-1200, USA*
[3] *Joint Institute for Heavy-Ion Research, Oak Ridge, Tennessee, 37831-6374, USA*
[4] *Department of Physics, P.O. Box 35 (YFL), FI-40014, University of Jyväskylä, Finland*
[5] *Physics Division, Oak Ridge National Laboratory, Oak Ridge, Tennessee 37831-6373, USA*
[6] *Institute of Theoretical Physics, University of Warsaw, ul. Hoża 69, PL-00-861, Warsaw, Poland*

(Dated: April 16, 2013)

Background: The major challenge for nuclear theory is to describe and predict global properties and collective modes of atomic nuclei. Of particular interest is the response of the nucleus to a time-dependent external field that impacts the low-energy multipole and beta-decay strength.

Purpose: We propose a method to compute low-lying collective modes in deformed nuclei within the finite amplitude method (FAM) based on the quasiparticle random-phase approximation (QRPA). By using the analytic property of the response function, we find the QRPA amplitudes by computing the residua of the FAM amplitudes by means of a contour integration around the QRPA poles in a complex frequency plane.

Methods: We use the superfluid nuclear density functional theory with Skyrme energy density functionals, FAM-QRPA approach, and the conventional matrix formulation of the QRPA (MQRPA).

Results: We demonstrate that the complex-energy FAM-QRPA method reproduces low-lying collective states obtained within the conventional matrix formulation of the QRPA theory. Illustrative calculations are performed for the isoscalar monopole strength in deformed ^{24}Mg and for low-lying $K = 0$ quadrupole vibrational modes of deformed Yb and Er isotopes.

Conclusions: The proposed FAM-QRPA approach allows one to efficiently calculate low-lying collective modes in spherical and deformed nuclei throughout the entire nuclear landscape, including shape-vibrational excitations, pairing vibrational modes, and beta-decay rates.

PACS numbers: 21.10.Re, 21.60.Jz, 23.20.Js

I. INTRODUCTION

Vibrational modes of atomic nuclei provide crucial information about nuclear structure. In particular, collective low-lying states contain information about the nucleonic shell structure, pairing correlations, and nuclear deformations [1, 2]. Giant resonances tell us about global properties of nuclear matter, such as compressibility and symmetry energy [3, 4]. Electromagnetic strength plays an important role in nuclear reactions involving photonuclear processes, including astrophysical reactions [5, 6] and the transmutation of nuclear waste [7].

The random-phase approximation (RPA) and its superfluid extension, the quasiparticle random-phase approximation (QRPA), are well-established microscopic theories describing excitations of many-body systems [1, 2]. QRPA can be viewed as a small-amplitude approximation of the time-dependent density functional theory [8, 9]. By using nuclear energy density functionals (EDFs) applicable to a large portion of the nuclear landscape, a variety of excited modes can be described by using QRPA.

Recently, there has been a considerable progress in the area of fully self-consistent QRPA calculations based on the nuclear density functional theory. Due to advances in high performance computing, deformed QRPA frameworks have been developed that can address properties of well-bound and loosely-bound nuclei [10–17].

The traditional QRPA methodology is based on a generalized eigenvalue problem involving a QRPA matrix containing the residual two-quasiparticle interaction. Because of a large number of quasiparticle states involved, the dimension of the QRPA matrix is typically quite large, especially when spherical symmetry is broken. This makes the problem computationally challenging. Therefore, in order to reduce the dimension of the two-quasiparticle basis, additional cutoffs are imposed on the configuration space of QRPA. Such truncations result in inconsistencies between the model spaces of Hartree-Fock-Bogoliubov (HFB) and QRPA calculations, and can result in breaking self-consistency and appearance of spurious modes [18].

To circumvent these problems, efficient methods to solve RPA have been formulated in the framework of the linear response theory and time-dependent HFB. One of these methods is the finite amplitude method (FAM) proposed in Ref. [19]. Within FAM, the strength function of an arbitrary one-body transition operator can be calculated without actually constructing and diagonalizing the full (Q)RPA matrix. Instead, the fields induced by the one-body transition (driving) operator are calculated and the linear response problem is solved iteratively. The practical implementation of the FAM requires minor extensions to the existing HFB codes to calculate

the induced fields and, therefore, is fairly straightforward. Systematic calculations with the FAM have been performed for the electric giant dipole resonances and low-lying dipole strength, illustrating computational advantages of the method [20, 21]. The FAM has also been extended to the superfluid systems, both spherical [22] and deformed [23].

Since the FAM equations are solved by introducing a small width, an imaginary part of the QRPA frequency, the method is very effective for describing excited modes in a region of high density of states. However, until now, a direct application of FAM to discrete low-lying excitations has not been fully accomplished. Quite recently, an efficient method to evaluate the QRPA matrix using FAM has been reported [24] that significantly reduces the computational effort, also enabling computations of low-lying discrete QRPA modes. A disadvantage of this approach is that a large memory is required to store the huge QRPA matrix, which subsequently needs to be diagonalized.

An alternative technique to solve the linear response problem is based on the iterative Arnoldi diagonalization method [25]. This method was first implemented for spherical systems without pairing and then further extended to spherical superfluid nuclei [26]. Because the Arnoldi diagonalization algorithm solves the QRPA eigenvalue problem in a smaller Krylov-space, the discrete excitations are within the scope of this method [27].

The goal of this work is to derive a method to calculate the discrete low-lying QRPA modes within the FAM framework. We shall refer to this new technique as FAM-QRPA in the following. Starting from the linear response theory, we show in Secs. II and III that a contour integration in the complex frequency plane around a QRPA root provides the QRPA eigenvectors. A similar technique was proposed in Ref. [28] to solve generalized eigenvalue problems. We devise several techniques to compute and assess the accuracy of QRPA modes. Next, in Sec. IV, we numerically demonstrate that the discrete FAM-QRPA solution for the low-lying states reproduces the modes obtained within the conventional matrix formulation of QRPA (MQRPA) and we apply FAM-QRPA to collective modes in deformed Er and Yb nuclei. Finally, the conclusions of our work are given in Sec. V.

II. FINITE AMPLITUDE METHOD

In this section we recapitulate the derivation of the FAM equations for superfluid systems following Sec. II of Ref. [22]. In the FAM formalism, the polarization of the system is induced by an external time-dependent field $\hat{F}(t)$ with a frequency ω:

$$\hat{F}(t) = \eta \left\{ \hat{F} e^{-i\omega t} + \hat{F}^\dagger e^{i\omega t} \right\}, \tag{1}$$

where

$$\hat{F} = \frac{1}{2} \sum_{\mu\nu} \left\{ F^{20}_{\mu\nu} \hat{\boldsymbol{A}}^\dagger_{\mu\nu} + F^{02}_{\mu\nu} \hat{\boldsymbol{A}}_{\mu\nu} + F^{11}_{\mu\nu} \hat{\boldsymbol{B}}_{\mu\nu} \right\}, \tag{2}$$

and $\hat{\boldsymbol{A}}^\dagger_{\mu\nu} = \hat{a}^\dagger_\mu \hat{a}^\dagger_\nu$ and $\hat{\boldsymbol{B}}_{\mu\nu} = \hat{a}^\dagger_\mu \hat{a}_\nu$ are two-quasiparticle operators. The parameter η is a (small) real number to expand particle and pair HFB densities to the first order. Contrary to Ref. [22], we assume that $\hat{F}$ is ω-independent in all applications in this work. However, our scheme can be easily extended to the case where $\hat{F}$ depends on ω.

The time-evolution of quasiparticle operators under the external field $\hat{F}(t)$ is determined by the time-dependent HFB (TDHFB) equation:

$$i\frac{\partial}{\partial t} \hat{a}_\mu(t) = [\hat{H}(t) + \hat{F}(t), \hat{a}_\mu(t)], \tag{3}$$

where time-dependent oscillation of quasiparticle operators is:

$$\hat{a}_\mu(t) = \{\hat{a}_\mu + \delta\hat{a}_\mu(t)\} e^{iE_\mu t}, \tag{4a}$$

$$\delta\hat{a}_\mu(t) = \eta \sum_\nu \hat{a}^\dagger_\nu \left\{ X_{\nu\mu}(\omega) e^{-i\omega t} + Y^*_{\nu\mu}(\omega) e^{i\omega t} \right\}, \tag{4b}$$

where E_μ is the one-quasiparticle energy and $X_{\mu\nu}(\omega)$ and $Y_{\mu\nu}(\omega)$ are the FAM amplitudes.

In terms of time-dependent quasiparticles, the TDHFB Hamiltonian can be written as $\hat{H}(t) = \hat{H}_0 + \delta\hat{H}(t)$, where:

$$\hat{H}_0 = \sum_\mu E_\mu \hat{\boldsymbol{B}}_{\mu\mu} \tag{5}$$

is the HFB Hamiltonian and

$$\delta\hat{H}(t) = \eta \left\{ \delta\hat{H}(\omega) e^{-i\omega t} + \delta\hat{H}^\dagger(\omega) e^{i\omega t} \right\} \tag{6}$$

with

$$\delta\hat{H}(\omega) = \frac{1}{2} \sum_{\mu\nu} \left\{ \delta H^{20}_{\mu\nu}(\omega) \hat{\boldsymbol{A}}^\dagger_{\mu\nu} + \delta H^{02}_{\mu\nu}(\omega) \hat{\boldsymbol{A}}_{\mu\nu} \right\} \tag{7}$$

represents a small-amplitude oscillation.

Inserting (1), (4), and (6) into (3) results in the FAM equations:

$$(E_\mu + E_\nu - \omega) X_{\mu\nu}(\omega) + \delta H^{20}_{\mu\nu}(\omega) = -F^{20}_{\mu\nu}, \tag{8a}$$

$$(E_\mu + E_\nu + \omega) Y_{\mu\nu}(\omega) + \delta H^{02}_{\mu\nu}(\omega) = -F^{02}_{\mu\nu}. \tag{8b}$$

By expanding $\delta H^{20}(\omega)$ and $\delta H^{02}(\omega)$ in terms of $X(\omega)$ and $Y(\omega)$, one obtains:

$$\delta H^{20}_{\mu\nu}(\omega) = \sum_{\mu'<\nu'} \{A_{\mu\nu,\mu'\nu'} - (E_\mu + E_\nu)\delta_{\mu\mu'}\delta_{\nu\nu'}\} X_{\mu'\nu'}(\omega) + \sum_{\mu'<\nu'} B_{\mu\nu,\mu'\nu'} Y_{\mu'\nu'}(\omega), \tag{9a}$$

$$\delta H^{02}_{\mu\nu}(\omega) = \sum_{\mu'<\nu'} \left\{A^*_{\mu\nu,\mu'\nu'} - (E_\mu + E_\nu)\delta_{\mu\mu'}\delta_{\nu\nu'}\right\} Y_{\mu'\nu'}(\omega) + \sum_{\mu'<\nu'} B^*_{\mu\nu,\mu'\nu'} X_{\mu'\nu'}(\omega), \tag{9b}$$

where A and B are the usual QRPA matrices [2]. The advantage of the FAM formulation is that the A and B matrices do not have to be computed explicitly. By substituting (9) into the FAM equations (8), the linear response equation becomes:

$$\left[\begin{pmatrix} A & B \\ B^* & A^* \end{pmatrix} - \omega \begin{pmatrix} 1 & 0 \\ 0 & -1 \end{pmatrix}\right] \begin{pmatrix} X(\omega) \\ Y(\omega) \end{pmatrix} = - \begin{pmatrix} F^{20} \\ F^{02} \end{pmatrix}, \quad (10)$$

where the sum over two quasiparticle space is restricted to quasiparticle indices $\mu < \nu$. The FAM equations are thus equivalent to the linear response formalism. Furthermore, the left hand side of (10) yields the QRPA equations when the right-hand side is set to zero. The FAM equations (8) are solved by using complex frequencies $\omega_\gamma = \omega + i\gamma$, where the imaginary part γ corresponds to a smearing width.

In terms of the FAM amplitudes $X(\omega_\gamma)$ and $Y(\omega_\gamma)$, the strength function $dB(\omega;F)/d\omega$ for the operator $\hat{F}$ can be written as:

$$\frac{dB(\omega;F)}{d\omega} = -\frac{1}{\pi}\mathrm{Im}S(F;\omega_\gamma), \quad (11)$$

$$S(F;\omega_\gamma) = \sum_{\mu<\nu} \left\{ F^{20*}_{\mu\nu} X_{\mu\nu}(\omega_\gamma) + F^{02*}_{\mu\nu} Y_{\mu\nu}(\omega_\gamma) \right\}. \quad (12)$$

III. FAM FOR DISCRETE QRPA MODES

The objective of this work is to formulate a FAM capable of describing low-lying discrete QRPA modes. We start by introducing the $2N \times 2N$ matrices [2]:

$$\mathcal{S} = \begin{pmatrix} A & B \\ B^* & A^* \end{pmatrix}, \mathcal{N} = \begin{pmatrix} 1 & 0 \\ 0 & -1 \end{pmatrix}, \mathcal{X} = \begin{pmatrix} X & Y^* \\ Y & X^* \end{pmatrix}, \quad (13)$$

where N is the dimension of the two-quasiparticle space, and the matrix elements $X^i_{\mu\nu}$ and $Y^i_{\mu\nu}$ of $\mathcal{X}$ are the QRPA amplitudes of the i-th mode with a positive eigenfrequency Ω_i. There also exists a counterpart QRPA solution (Y^{i*}, X^{i*}) with a negative eigenfrequency $-\Omega_i$. We assume here that all the QRPA frequencies are real, that is, $\mathcal{S}$ is positive definite. In terms of matrices (13), the QRPA equation can be expressed as:

$$\mathcal{S}\mathcal{X} = \mathcal{N}\mathcal{X}\mathcal{O}, \quad (14)$$

where $\mathcal{O}$ is a $2N \times 2N$ diagonal matrix containing the QRPA eigenfrequencies $(\Omega_1, \ldots, \Omega_N, -\Omega_1, \ldots, -\Omega_N)$. The orthonormalization condition for the QRPA eigenvectors is:

$$\mathcal{X}\mathcal{N}\mathcal{X}^\dagger = \mathcal{N}. \quad (15)$$

By applying Eqs. (14) and (15), the matrix on the left-hand side of (10) can be inverted, which yields the FAM amplitudes [2]:

$$\begin{aligned} \begin{pmatrix} X(\omega_\gamma) \\ Y(\omega_\gamma) \end{pmatrix} &= -R(\omega_\gamma) \begin{pmatrix} F^{20} \\ F^{02} \end{pmatrix} \\ &= -\mathcal{X}(\mathcal{O} - \omega_\gamma \mathcal{I})^{-1} \mathcal{N}\mathcal{X}^\dagger \begin{pmatrix} F^{20} \\ F^{02} \end{pmatrix}, \end{aligned} \quad (16)$$

where $\mathcal{I}$ is a $2N \times 2N$ unit matrix and $R(\omega_\gamma)$ is the response function. The explicit form of $R(\omega_\gamma)$ is:

$$R_{\mu\nu\mu'\nu'}(\omega_\gamma) = \sum_i \begin{bmatrix} \dfrac{X^i_{\mu\nu}X^{i*}_{\mu'\nu'}}{\Omega_i - \omega_\gamma} + \dfrac{Y^{i*}_{\mu\nu}Y^i_{\mu'\nu'}}{\Omega_i + \omega_\gamma} & \dfrac{X^i_{\mu\nu}Y^{i*}_{\mu'\nu'}}{\Omega_i - \omega_\gamma} + \dfrac{Y^{i*}_{\mu\nu}X^i_{\mu'\nu'}}{\Omega_i + \omega_\gamma} \\ \dfrac{Y^i_{\mu\nu}X^{i*}_{\mu'\nu'}}{\Omega_i - \omega_\gamma} + \dfrac{X^{i*}_{\mu\nu}Y^i_{\mu'\nu'}}{\Omega_i + \omega_\gamma} & \dfrac{Y^i_{\mu\nu}Y^{i*}_{\mu'\nu'}}{\Omega_i - \omega_\gamma} + \dfrac{X^{i*}_{\mu\nu}X^i_{\mu'\nu'}}{\Omega_i + \omega_\gamma} \end{bmatrix}. \quad (17)$$

Substitution of Eq. (17) into Eq. (16) provides the relation between the FAM amplitudes and QRPA amplitudes

$$X_{\mu\nu}(\omega_\gamma) = -\sum_i \left\{ \frac{X^i_{\mu\nu}\langle i|\hat{F}|0\rangle}{\Omega_i - \omega_\gamma} + \frac{Y^{i*}_{\mu\nu}\langle 0|\hat{F}|i\rangle}{\Omega_i + \omega_\gamma} \right\}, \quad (18a)$$

$$Y_{\mu\nu}(\omega_\gamma) = -\sum_i \left\{ \frac{Y^i_{\mu\nu}\langle i|\hat{F}|0\rangle}{\Omega_i - \omega_\gamma} + \frac{X^{i*}_{\mu\nu}\langle 0|\hat{F}|i\rangle}{\Omega_i + \omega_\gamma} \right\}, \quad (18b)$$

where

$$\begin{aligned} \langle i|\hat{F}|0\rangle &= \langle \Phi_0|[\hat{O}_i, \hat{F}]|\Phi_0\rangle \\ &= \sum_{\mu<\nu} (X^{i*}_{\mu\nu}F^{20}_{\mu\nu} + Y^{i*}_{\mu\nu}F^{02}_{\mu\nu}), \end{aligned} \quad (19)$$

$$\begin{aligned} \langle 0|\hat{F}|i\rangle &= \langle \Phi_0|[\hat{O}^\dagger_i, \hat{F}]|\Phi_0\rangle \\ &= \sum_{\mu<\nu} (F^{02}_{\mu\nu}X^i_{\mu\nu} + F^{20}_{\mu\nu}Y^i_{\mu\nu}), \end{aligned} \quad (20)$$

are the QRPA transition strengths between the QRPA ground state $|0\rangle$ and i-th excited state $|i\rangle$, $|\Phi_0\rangle$ is the

HFB state, the operator:

$$\hat{O}_i^\dagger = \sum_{\mu<\nu} \{X^i_{\mu\nu}\hat{\boldsymbol{A}}^\dagger_{\mu\nu} - Y^i_{\mu\nu}\hat{\boldsymbol{A}}_{\mu\nu}\} \tag{21}$$

is the QRPA phonon operator, and $X^i_{\mu\nu}$ and $Y^i_{\mu\nu}$ are the QRPA amplitudes of a state i.

Equation (18) shows that the FAM amplitudes $X(\omega_\gamma)$ and $Y(\omega_\gamma)$ have first-order poles on the real axis at $\omega_\gamma = \Omega_i$ and $-\Omega_i$. By calculating the standard FAM strength function, approximate positions of the poles of the low-lying states of interest can be located. This allows one to define a closed contour C_i in the complex energy plane that encloses the i-th positive pole Ω_i. According to Cauchy's integral formula, the contour integration of the FAM amplitudes (18) along C_i gives the residue at the i-th pole:

$$\frac{1}{2\pi i}\oint_{C_i} X_{\mu\nu}(\omega_\gamma)d\omega_\gamma = \mathrm{Res}(X_{\mu\nu},\Omega_i) = X^i_{\mu\nu}\langle i|\hat{F}|0\rangle, \tag{22a}$$

$$\frac{1}{2\pi i}\oint_{C_i} Y_{\mu\nu}(\omega_\gamma)d\omega_\gamma = \mathrm{Res}(Y_{\mu\nu},\Omega_i) = Y^i_{\mu\nu}\langle i|\hat{F}|0\rangle. \tag{22b}$$

The absolute value of the transition strength for the i-th QRPA mode can then be expressed as:

$$|\langle i|\hat{F}|0\rangle|^2 = \sum_{\mu<\nu}\left\{\left|\frac{1}{2\pi i}\oint_{C_i} X_{\mu\nu}(\omega_\gamma)d\omega_\gamma\right|^2 - \left|\frac{1}{2\pi i}\oint_{C_i} Y_{\mu\nu}(\omega_\gamma)d\omega_\gamma\right|^2\right\}, \tag{23}$$

where we have used the normalization condition (15) for the QRPA amplitudes. The individual QRPA amplitudes $X^i_{\mu\nu}$ and $Y^i_{\mu\nu}$ can thus be calculated as:

$$X^i_{\mu\nu} = e^{-i\theta}|\langle i|\hat{F}|0\rangle|^{-1}\frac{1}{2\pi i}\oint_{C_i} X_{\mu\nu}(\omega_\gamma)d\omega_\gamma, \tag{24a}$$

$$Y^i_{\mu\nu} = e^{-i\theta}|\langle i|\hat{F}|0\rangle|^{-1}\frac{1}{2\pi i}\oint_{C_i} Y_{\mu\nu}(\omega_\gamma)d\omega_\gamma. \tag{24b}$$

The common phase $e^{i\theta} = \langle i|\hat{F}|0\rangle/|\langle i|\hat{F}|0\rangle|$ cannot be determined and remains arbitrary.

The information about the exact value of the QRPA eigenfrequency is not necessary to perform the contour integration as long as the corresponding pole is located inside the contour. However, it can be calculated from the integration of the induced fields. Indeed, from Eqs. (9) and (14), one obtains:

$$\frac{1}{2\pi i}\oint_{C_i} \delta H^{20}_{\mu\nu}(\omega_\gamma)d\omega_\gamma = \langle i|\hat{F}|0\rangle X^i_{\mu\nu}\left\{\Omega_i - (E_\mu + E_\nu)\right\}, \tag{25a}$$

$$\frac{1}{2\pi i}\oint_{C_i} \delta H^{02}_{\mu\nu}(\omega_\gamma)d\omega_\gamma = \langle i|\hat{F}|0\rangle Y^i_{\mu\nu}\left\{-\Omega_i - (E_\mu + E_\nu)\right\}. \tag{25b}$$

These $2N$ equations can be used to compute Ω_i, but this method is prone to large numerical errors when amplitudes $X^i_{\mu\nu}$ or $Y^i_{\mu\nu}$ are very small. To this end, a better way of determining the QRPA eigenfrequencies is through an expression derived from Eq. (25):

$$\Omega_i^2 = \sum_{\mu<\nu}(|\Omega_i X^i_{\mu\nu}|^2 - |\Omega_i Y^i_{\mu\nu}|^2) = \frac{1}{|\langle i|\hat{F}|0\rangle|^2}\sum_{\mu<\nu} \left\{\left|\frac{1}{2\pi i}\oint_{C_i}\left((E_\mu+E_\nu)X_{\mu\nu}(\omega_\gamma) + \delta H^{20}_{\mu\nu}(\omega_\gamma)\right)d\omega_\gamma\right|^2 - \left|\frac{1}{2\pi i}\oint_{C_i}\left((E_\mu+E_\nu)Y_{\mu\nu}(\omega_\gamma) + \delta H^{02}_{\mu\nu}(\omega_\gamma)\right)d\omega_\gamma\right|^2\right\}. \tag{26}$$

The formalism presented above allows one to establish an explicit connection between the FAM strength function and the smeared QRPA strength function. By substituting Eq. (18) into Eq. (12) we obtain:

$$S(F,\omega_\gamma) = -\sum_i\left(\frac{|\langle i|\hat{F}|0\rangle|^2}{\Omega_i - \omega - i\gamma} + \frac{|\langle i|\hat{F}|0\rangle|^2}{\Omega_i + \omega + i\gamma}\right), \tag{27}$$

$$\frac{dB}{d\omega}(F,\omega) = -\frac{1}{\pi}\mathrm{Im}S(F,\omega_\gamma) = \frac{\gamma}{\pi}\sum_i\left\{\frac{|\langle i|\hat{F}|0\rangle|^2}{(\Omega_i-\omega)^2+\gamma^2} - \frac{|\langle i|\hat{F}|0\rangle|^2}{(\Omega_i+\omega)^2+\gamma^2}\right\}. \tag{28}$$

According to Eq. (27), the discrete QRPA transition strength can be directly computed from the FAM strength function (12):

$$|\langle i|\hat{F}|0\rangle|^2 = \frac{1}{2\pi i}\oint_{C_i} S(F,\omega)d\omega\,. \tag{29}$$

In summary, as discussed above, there exist several techniques, based on the residue at the QRPA pole, to calculate discrete transition strengths within the FAM-QRPA formalism:

A: The contour integration of the FAM amplitudes $X_{\mu\nu}(\omega)$ and $Y_{\mu\nu}(\omega)$ as in Eq. (23);

B: The contour integration of the FAM strength function as in Eq. (29);

C: Individual QRPA amplitudes $X^i_{\mu\nu}$ and $Y^i_{\mu\nu}$ can be found using (24) to obtain the transition matrix element (19);

D: The QRPA amplitudes $X^i_{\mu\nu}$ and $Y^i_{\mu\nu}$ found with technique C are independent of the choice of the external field used in FAM-QRPA. Therefore, for example, the isoscalar strength associated with the field $\hat{F}'$ can be computed using the QRPA amplitudes obtained in FAM-QRPA with the isovector external field $\hat{F}$.

Although all of these strategies are formally equivalent, the technique B is the easiest to implement in the current FAM codes. By virtue of D, once the discrete QRPA amplitudes have been found for a given state, they can be used to calculate a transition matrix element for any transition operator.

If assigned incorrectly, the integration contour C' could include secondary unwanted poles. (For example, there could be two states: a collective one carrying a strong transition strength and a nearby-lying non-collective one with a negligible contribution to the total transition strength.) Since the FAM amplitudes $X_{\mu\nu}(\omega)$ and $Y_{\mu\nu}(\omega)$ (18) are sums of the residua, the right hand side of Eq. (22) contains contributions from all the poles included inside C'. The calculated transition strength then becomes:

$$B(C';F) = \sum_{i\in C'} |\langle i|\hat{F}|0\rangle|^2. \tag{30}$$

Because of the orthogonality of QRPA amplitudes $X^i_{\mu\nu}$ and $Y^i_{\mu\nu}$, the interference terms between different states cancel out. Therefore, if C' encircles two or more poles, the transition strengths from all those poles contribute to the total strength without the interference term when techniques A and B are used. Within C, calculated discrete amplitudes $X^i_{\mu\nu}$ and $Y^i_{\mu\nu}$ contain a mixture of all states inside the contour. However, when applied to Eq. (19), the same transition strength as with techniques A and B is obtained. However, in the method D, due to the incorrect amplitudes $X^i_{\mu\nu}$ and $Y^i_{\mu\nu}$, the final strength

$$B_{\rm D}(C';F') = \frac{|\sum_{i\in C'}\langle i|\hat{F}'|0\rangle\langle i|\hat{F}|0\rangle^*|^2}{\sum_{i\in C'}|\langle i|\hat{F}|0\rangle|^2}, \tag{31}$$

would be incorrect.

As will be demonstrated in Sec. IV, we have checked numerically that when the contour includes multiple poles, techniques A-C indeed yield the total summed strength while D does not. This apparent deficiency of D can be used to our advantage to verify that the selected contour C_i includes only one pole.

One can also find a clue to correct the assignment of the contour by calculating the QRPA eigenfrequency Ω^2 using Eq. (26):

$$\Omega^2_{C'} = \sum_{i\in C'}\left(|\langle i|\hat{F}|0\rangle|^2\Omega_i^2\right) / \sum_{i\in C'}|\langle i|\hat{F}|0\rangle|^2. \tag{32}$$

When the contour encloses one collective and one non-collective QRPA root with respect to an external field $\hat{F}$, Eq. (26) yields the approximate energy of the collective state.

IV. NUMERICAL RESULTS

To validate the FAM-QRPA formalism discussed in the previous section, we carried out numerical computations using the FAM framework developed in Ref. [23] to evaluate the transition strength and the corresponding residua. Our FAM-QRPA method is based on the HFB code HFBTHO [29, 30], which solves the Skyrme-HFB equations in the (transformed) harmonic oscillator basis assuming axial and mirror symmetries. The FAM equations are solved iteratively by using the modified Broyden's procedure [31, 32], which offers a rapid and stable convergence, which weakly depends on the magnitude of the imaginary frequency γ.

A. Test case: monopole strength in ^{24}Mg

To compare with full MQRPA, we consider the same case of the monopole strength in ^{24}Mg as discussed in Ref. [23]. We use SLy4 Skyrme EDF [33] and a contact volume pairing with a 60 MeV quasiparticle energy cutoff and the pairing strength $V_0 = -125.20\,\text{MeV fm}^{-3}$ for both neutrons and protons. In order to perform exact comparison without any truncation at the MQRPA level, we take the single-particle basis consisting of $N_{\rm sh} = 5$ oscillator shells [23].

The oblate-deformed HFB minimum of ^{24}Mg was obtained at the quadrupole mass deformation $\beta = -0.163$. In this configuration, both neutrons and protons are in the superfluid phase, with pairing gaps $\Delta_{\rm n} = 0.666\,\text{MeV}$ and $\Delta_{\rm p} = 0.654\,\text{MeV}$, respectively. In the FAM calculation, we used the value of the parameter $\eta = 10^{-7}$, which was found to provide the best accuracy [23]. For the convergence criterion of FAM iterations, defined in terms of the maximum difference between collective FAM amplitudes in two consecutive iterations, we used the value of 10^{-5}; this accuracy is typically reached after about 40 iterations.

As for $\hat{F}$, we consider the isoscalar monopole (ISM) and isovector monopole (IVM) operators:

$$\hat{F}^{\rm ISM} = \frac{eZ}{A}\sum_{i=1}^{A} r_i^2, \tag{33a}$$

$$\hat{F}^{\rm IVM} = \frac{eZ}{A}\sum_{i=1}^{N} r_i^2 - \frac{eN}{A}\sum_{i=1}^{Z} r_i^2. \tag{33b}$$

For the integration contours we take circles with radii 0.02 MeV, centered close to MQRPA frequencies. The contour integration is discretized with 11 points, unless stated otherwise.

Figure 1 shows the isoscalar monopole strength function at the oblate configuration of ^{24}Mg calculated with the conventional FAM by using three values of γ. The strength function obtained with $\gamma = 0.5\,\text{MeV}$ shows a very smooth distribution with the broad bumps carrying the largest strength. By going to smaller values of γ, one reveals the detailed structure of QRPA modes. For example, to separate the smaller first peak at $\Omega_1 = 1.32\,\text{MeV}$ from the second one at $\Omega_2 = 1.37\,\text{MeV}$, a very small γ – of the order of 1 keV – is required.

TABLE I. Low-lying $K = 0$ QRPA energies Ω_i and isoscalar monopole strength $|\langle i|\hat{F}|0\rangle|^2$ calculated with MQRPA and FAM-QRPA for the oblate configuration of ^{24}Mg. All the modes with $\Omega_i < 7.5$ MeV are listed. The transition strength was computed using the techniques A-D described in Sec. III. The isoscalar monopole strength FAM-D is calculated from the FAM-QRPA amplitudes generated by the external isovector monopole field. The numbers in parentheses denote powers of 10.

Ω_i (MeV)		$\lvert\langle i\rvert\hat{F}^{\rm ISM}\lvert 0\rangle\rvert^2$ (e^2 fm^4)				
MQRPA	FAM	MQRPA	FAM-A	FAM-B	FAM-C	FAM-D
1.3185	1.3183	5.729(-4)	5.771(-4)	5.773(-4)	5.776(-4)	5.781(-4)
1.3731	1.3731	1.539(-2)	1.511(-2)	1.511(-2)	1.510(-2)	1.511(-2)
2.4582	2.4581	0.1796	0.1780	0.1782	0.1784	0.1783
2.5998	2.5975	2.957(-3)	3.056(-3)	3.058(-3)	3.060(-3)	3.057(-3)
3.6687	3.6657	0.5776	0.5755	0.5771	0.5788	0.5788
5.1185	5.1212	3.539(-4)	3.744(-4)	4.040(-4)	4.360(-4)	4.345(-4)
7.4108	7.4084	0.4900	0.4820	0.4834	0.4848	0.4848

TABLE II. Similar as in Table I but for the isovector monopole modes.

Ω_i (MeV)		$\lvert\langle i\rvert\hat{F}^{\rm IVM}\lvert 0\rangle\rvert^2$ (e^2 fm^4)				
MQRPA	FAM	MQRPA	FAM-A	FAM-B	FAM-C	FAM-D
1.3185	1.3183	1.557(-3)	1.547(-3)	1.547(-3)	1.547(-3)	1.547(-3)
1.3731	1.3731	5.771(-5)	5.810(-5)	5.818(-5)	5.827(-5)	5.824(-5)
2.4582	2.4581	1.968(-6)	1.643(-6)	1.896(-6)	2.188(-6)	2.047(-6)
2.5998	2.5975	8.978(-5)	8.870(-5)	8.894(-5)	8.919(-5)	8.907(-5)
3.6687	3.6657	1.555(-5)	8.681(-6)	1.140(-5)	1.498(-5)	1.515(-5)
5.1185	5.1212	3.907(-2)	3.885(-2)	3.899(-2)	3.914(-2)	3.914(-2)
7.4108	7.4084	1.388(-5)	2.926(-5)	2.228(-5)	1.697(-5)	1.622(-5)

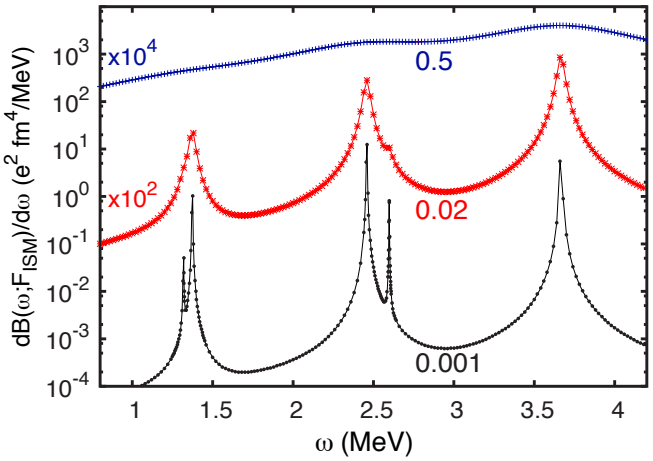

FIG. 1. (Color online) The low-lying isoscalar monopole strength at the oblate HFB minimum of ^{24}Mg calculated with the conventional FAM-QRPA using three values of smearing width γ (in MeV).

In Tables I and II we show the energies and transition strength of the low-lying $K = 0$ QRPA modes, calculated with MQRPA and FAM. Although the centers of the contours in the complex ω_γ-plane are only approximately chosen, the low-lying QRPA eigenfrequencies calculated with FAM are in good agreement with MQRPA results. The agreement is excellent for the lowest-lying states, which are usually of more interest. The FAM transition strength was obtained using the techniques A-D described in Sec. III. It is gratifying to see that the four methods generally agree at least up to two decimal places, except for the modes carrying very small strength ($\sim 10^{-4}\, e^2$fm^4). The nice agreement between FAM-C and FAM-D results demonstrates the consistency between the two sets of QRPA amplitudes calculated from the isoscalar and isovector external monopole fields. The difference between the strengths obtained by the MQRPA and FAM is consistent with the convergence criteria used in the FAM iterations.

Figure 2 demonstrates the convergence of the QRPA amplitudes against the number of discretization points $N_{\rm disc}$ used in the contour integration. Specifically, it shows the orthogonality of the QRPA amplitudes for the three lowest QRPA states. The orthogonality between the first and third state, and between the second and third state, is achieved already at $N_{\rm disc} = 4$, while the convergence for the pair of first and second states is slower. This is not surprising as the energies of the first and second QRPA roots differs only by 0.05 MeV; hence, and a finer integration mesh is required to remove the contribution from the unwanted pole outside of the contour. Our results show that to obtain the convergence for the contour integration, consistent with the accuracy required during the regular FAM iterations, taking 11 points is fully sufficient, at least for the two lowest modes.

Lastly, we discuss an example of an incorrect contour assignment following the discussion in Sec. III. A contour of radius of 0.2 MeV, centered at 1.3 MeV, includes

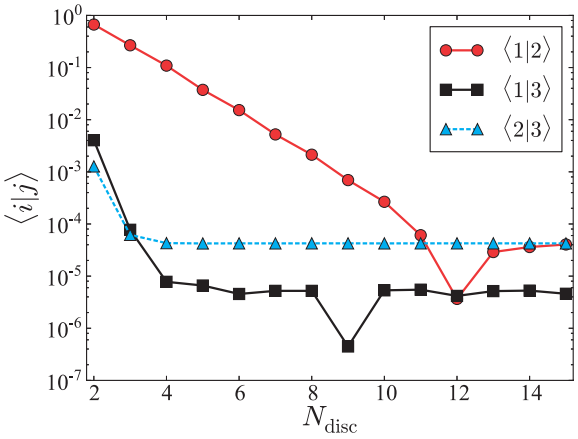

FIG. 2. (Color online) Convergence of the orthogonality of the states as a number of discretization points of a circular contour with radius 0.02 MeV. The first three low-lying states labeled as 1 (1.32 MeV), 2 (1.37 MeV), and 3 (2.46 MeV) are shown.

the first two QRPA solutions at 1.32 MeV and 1.37 MeV. Such an incorrect choice would be made if the contour were determined from the isoscalar strength function calculated with a resolution of $\gamma = 0.02$ MeV shown in Fig. 1. The calculated isoscalar (isovector) monopole transition strength determined according to A-C is 1.57×10^{-2} (1.61×10^{-3}) $e^2\,\mathrm{fm}^4$, which is precisely the sum of the two QRPA strengths. However, method D completely fails, yielding the values of $6\times 10^{-8}\,e^2\,\mathrm{fm}^4$ (isoscalar) and $3\times 10^{-9}\,e^2\,\mathrm{fm}^4$ (isovector), that are clearly off from those obtained with the procedures A-C. The QRPA frequency calculated from Eq. (26) with the isoscalar (isovector) monopole external field is 1.371 MeV (1.320 MeV). Since the isoscalar (isovector) monopole strength of the second (first) QRPA state is larger than that of the first (second) QRPA state by two orders of magnitude, the QRPA frequency calculated using the contour, which encloses both poles, is close to the energy of the collective state. Therefore, the consistency between the results obtained in methods C and D, together with the value of weighted frequency, can be used to find the contour that encloses a single QRPA pole.

B. Low-lying QRPA modes in deformed rare-earth nuclei

To demonstrate the feasibility of the FAM-QRPA formalism to describe the low-lying collective modes of deformed nuclei, we have performed FAM calculations for the low-lying $K = 0$ strength of ^{166,168,172}Yb, and ^{170}Er, which were previously studied with MQRPA in Refs. [12, 13]. The calculations were carried out using SkM* Skyrme EDF [34] with the volume pairing. The pairing strengths have been adjusted to reproduce the odd-even binding energy difference in ^{172}Yb evaluated with the three-point expression. They are: $V_{\rm n} = -176\,\mathrm{MeV\,fm}^{-3}$ and $V_{\rm p} = -218\,\mathrm{MeV\,fm}^{-3}$ for the quasiparticle energy cutoff $E_{\rm cut} = 60$ MeV and $V_{\rm n} = -150\,\mathrm{MeV\,fm}^{-3}$ and $V_{\rm p} = -177.5\,\mathrm{MeV\,fm}^{-3}$ for $E_{\rm cut} = 200$ MeV. To obtain QRPA amplitudes in FAM, we applied the isoscalar quadrupole $K = 0$ external field [18], and the electric reduced matrix elements $B(E2)$ for the excitational modes discussed in Refs. [12, 13] are computed using the technique D described in Sec. III. The transformed harmonic oscillator basis with 20 major oscillator shells was employed. To compute residua, we used the circular contours with radii 0.1 MeV for ^{166}Yb, ^{172}Yb, and ^{170}Er, and with radii 0.01 MeV for ^{168}Yb. The locations of the contour centers estimated from the conventional FAM calculations are: 1.40 MeV, 1.75 MeV, 1.30 MeV, and 1.30 MeV for ^{166}Yb, ^{168}Yb, ^{172}Yb, and ^{170}Er, respectively. The results were compared with the MQRPA calculations of Refs. [12, 13] employing a different HFB solver and an additional cutoff associated with the occupation probabilities of canonical states.

TABLE III. FAM-QRPA energies and $B(E2)$ values of the low-lying $K = 0$ states in ^{166}Yb, ^{168}Yb, ^{172}Yb, and ^{170}Er at $E_{\rm cut} = 200$ MeV compared to the MQRPA results of Ref. [13]. The additional result for ^{172}Yb corresponding $E_{\rm cut} = 60$ MeV is compared to the MQRPA values obtained in Ref. [12].

nucleus	Ω_i (MeV)		$B(E2)$ (e^2b^2)	
	MQRPA	FAM	MQRPA	FAM
^{166}Yb	1.802	1.422	0.0398	0.0327
^{168}Yb	2.039	1.747	0.0343	0.0186
^{172}Yb	1.605	1.306	0.0049	0.0088
^{170}Er	1.596	1.322	0.0030	0.0047
^{172}Yb[a]	1.390	1.319	0.0050	0.0092

[a] $E_{\rm cut} = 60$ MeV

Table III displays the results for excitation energies and $B(E2)$ rates of the $K = 0$ QRPA modes. For ^{172}Yb the calculations were carried out with two quasiparticle cutoffs: $E_{\rm cut} = 60$ MeV and 200 MeV. The FAM-QRPA excitation energy is close to the MQRPA value with $E_{\rm cut} = 60$ MeV [12], but this agreement does not hold when $E_{\rm cut}$ is increased. Indeed, while our FAM-QRPA values weakly depend on $E_{\rm cut}$, a 15% increase of the MQRPA energy for ^{172}Yb was reported in Ref. [13] when going to $E_{\rm cut} = 200$ MeV. Interestingly, the $B(E2)$ values weakly depend on energy cutoff in both methods. However, the $B(E2)$ values obtained in FAM-QRPA are twice as large as the MQRPA results.

For ^{166}Yb, ^{168}Yb, and ^{170}Er, the excitation energies obtained in MQRPA are larger by 0.3-0.4 MeV than those in FAM-QRPA. The agreement between $B(E2)$ values is good in ^{166}Yb, but gets worse in the other cases studied. It is difficult to speculate what is the origin of those differences. We note, however, that (i) the HFB solvers used in both calculations are different (see benchmarking results in Ref. [35]), and (ii) there are additional canonical energy cutoffs in in MQRPA [18] that are not present

in our FAM-QRPA method.

TABLE IV. Isoscalar and isovector quadrupole strength (in $e^2\,\mathrm{fm}^4$) of the low-lying $K = 0$ states in ^{166}Yb, ^{168}Yb, ^{172}Yb, and ^{170}Er shown in Table III with $E_{\mathrm{cut}} = 200\,\mathrm{MeV}$. The isoscalar (isovector) strength in FAM-C is calculated using the isoscalar (isovector) quadrupole external field. The isoscalar (isovector) quadrupole strength in FAM-D is calculated using the QRPA amplitudes obtained from the FAM calculation using the isovector (isoscalar) quadrupole external field.

nucleus	ISQ		IVQ	
	FAM-C	FAM-D	FAM-C	FAM-D
^{166}Yb	299.854	299.856	0.585519	0.585520
^{168}Yb	160.126	160.127	0.969114	0.969124
^{172}Yb	93.2710	93.2735	0.081406	0.081404
^{170}Er	56.2932	56.2913	0.460285	0.460254

The isoscalar quadrupole (ISQ) and isovector quadrupole (IVQ) strengths are displayed in Table IV for the deformed nuclei shown in Table III. The strengths obtained from the QRPA amplitudes derived from two external quadrupole fields agree excellently. This result clearly shows that the contours used in these calculations enclose only a single QRPA pole.

V. CONCLUSIONS

We have formulated and tested the FAM-QRPA method for efficient computations of discrete QRPA modes. The new framework is based on the application of Cauchy's integral formula to the FAM amplitudes defined in the complex frequency plane. The method is fully self-consistent and does not require any configuration-space truncations at the QRPA level. The method is particularly useful when applied to the isolated collective QRPA modes. For the description of the transition strength carried by densely distributed modes, the conventional FAM formulation is more appropriate.

The FAM-QRPA method has been benchmarked and tested by comparing with MQRPA results for an oblate configuration of ^{24}Mg. Illustrative examples of large-scale calculations have been presented for the $K = 0$ isoscalar and isovector quadrupole modes of deformed rare-earth nuclei ^{166}Yb, ^{168}Yb, ^{172}Yb, and ^{170}Er.

Our results demonstrate that the proposed formulation of FAM-QRPA can be used as an efficient tool to calculate discrete QRPA modes of heavy, deformed, and superfluid nuclei. Once the contour around the mode of interest is specified, the FAM-QRPA method allows one to perform a fully self-consistent QRPA calculation employing *the same* model space as in HFB. Thanks to the rapid convergence achieved with Broyden's method used in our implementation, FAM-QRPA is amenable to high-performance parallel computing. This offers promise of systematic calculations of various kinds of low-lying excitations and decays over the entire nuclear landscape. Of particular importance are QRPA studies of low-energy dipole and quadrupole states, β decays, and $\beta\beta$ decays. The work on extending the FAM-QRPA formalism to $K \neq 0$ and charge-exchange modes is in progress.

ACKNOWLEDGMENTS

Useful discussions with J. Dobaczewski and T. Nakatsukasa are gratefully acknowledged. This work was supported by the U.S. Department of Energy under Contract Nos. DE-FG02-96ER40963 (University of Tennessee), de-sc0008499 (NUCLEI SciDAC Collaboration), by JUSTIPEN (Japan-U.S. Theory Institute for Physics with Exotic Nuclei) under grant number No. DEFG02-06ER41407 (University of Tennessee), by the Academy of Finland under the Centre of Excellence Programme 2012–2017 (Nuclear and Accelerator Based Physics Programme at JYFL), and FIDIPRO programme. An award of computer time was provided by the Innovative and Novel Computational Impact on Theory and Experiment (INCITE) program.

[1] A. Bohr and B. Mottelson, *Nuclear Structure, Vol. II* (W A. Benjamin, Reading, MA, 1975).
[2] P. Ring and P. Schuck, *The Nuclear Many-Body Problem* (Springer-Verlag, 1980).
[3] E. Lipparini and S. Stringari, Phys. Rep. **175**, 103 (1989).
[4] M. N. Harakeh and A. van der Woude, *Giant Resonances: Fundamental High-Frequency Modes of Nuclear Excitation* (Oxford University Press, 2001).
[5] M. Arnould, S. Goriely, and K. Takahashi, Phys. Rep. **450**, 97 (2007).
[6] I. Daoutidis and S. Goriely, Phys. Rev. C **86**, 034328 (2012).
[7] M. Beard, S. Frauendorf, B. Kämpfer, R. Schwengner, and M. Wiescher, Phys. Rev. C **85**, 065808 (2012).
[8] J.-P. Blaizot and G. Ripka, *Quantum Theory of Finite Systems* (MIT Press, Cambridge, 1986).
[9] T. Nakatsukasa, Prog. Theor. Exp. Phys. **2012**, 01A207 (2012).
[10] K. Yoshida, Phys. Rev. C **82**, 034324 (2010).
[11] K. Yoshida and T. Nakatsukasa, Phys. Rev. C **83**, 021304 (2011).
[12] J. Terasaki and J. Engel, Phys. Rev. C **82**, 034326 (2010).
[13] J. Terasaki and J. Engel, Phys. Rev. C **84**, 014332 (2011).
[14] C. Losa, A. Pastore, T. Døssing, E. Vigezzi, and R. A. Broglia, Phys. Rev. C **81**, 064307 (2010).
[15] S. Péru, G. Gosselin, M. Martini, M. Dupuis, S. Hilaire, and J.-C. Devaux, Phys. Rev. C **83**, 014314 (2011).
[16] S. Péru and H. Goutte, Phys. Rev. C **77**, 044313 (2008).

[17] M. Martini, S. Péru, and M. Dupuis, Phys. Rev. C **83**, 034309 (2011).
[18] J. Terasaki, J. Engel, M. Bender, J. Dobaczewski, W. Nazarewicz, and M. Stoitsov, Phys. Rev. C **71**, 034310 (2005).
[19] T. Nakatsukasa, T. Inakura, and K. Yabana, Phys. Rev. C **76**, 024318 (2007).
[20] T. Inakura, T. Nakatsukasa, and K. Yabana, Phys. Rev. C **80**, 044301 (2009).
[21] T. Inakura, T. Nakatsukasa, and K. Yabana, Phys. Rev. C **84**, 021302 (2011).
[22] P. Avogadro and T. Nakatsukasa, Phys. Rev. C **84**, 014314 (2011).
[23] M. Stoitsov, M. Kortelainen, T. Nakatsukasa, C. Losa, and W. Nazarewicz, Phys. Rev. C **84**, 041305 (2011).
[24] P. Avogadro and T. Nakatsukasa, Phys. Rev. C **87**, 014331 (2013).
[25] J. Toivanen, B. G. Carlsson, J. Dobaczewski, K. Mizuyama, R. R. Rodríguez-Guzmán, P. Toivanen, and P. Veselý, Phys. Rev. C **81**, 034312 (2010).
[26] P. Veselý, J. Toivanen, B. G. Carlsson, J. Dobaczewski, N. Michel, and A. Pastore, Phys. Rev. C **86**, 024303 (2012).
[27] B. G. Carlsson, J. Toivanen, and A. Pastore, Phys. Rev. C **86**, 014307 (2012).
[28] T. Sakurai and H. Sugiura, J. Comput. Appl. Math **159**, 119 (2003).
[29] M. Stoitsov, J. Dobaczewski, W. Nazarewicz, and P. Ring, Comp. Phys. Comm. **167**, 43 (2005).
[30] M. Stoitsov, N. Schunck, M. Kortelainen, N. Michel, H. Nam, E. Olsen, J. Sarich, and S. Wild, Comp. Phys. Comm. **184**, 1592 (2013).
[31] D. D. Johnson, Phys. Rev. B **38**, 12807 (1988).
[32] A. Baran, A. Bulgac, M. M. Forbes, G. Hagen, W. Nazarewicz, N. Schunck, and M. V. Stoitsov, Phys. Rev. C **78**, 014318 (2008).
[33] E. Chabanat, P. Bonche, P. Haensel, J. Meyer, and R. Schaeffer, Nucl. Phys. A **635**, 231 (1998).
[34] J. Bartel, P. Quentin, M. Brack, C. Guet, and H.-B. Håkansson, Nucl. Phys. A **386**, 79 (1982).
[35] J. C. Pei, M. V. Stoitsov, G. I. Fann, W. Nazarewicz, N. Schunck, and F. R. Xu, Phys. Rev. C **78**, 064306 (2008).